Squaring the Circle in Peptide Assembly: From Fibers to Discrete Nanostructures by *de Novo* Design

Aimee L. Boyle,[†] Elizabeth H. C. Bromley,*[,†,#] Gail J. Bartlett,[†] Richard B. Sessions,[‡]
Thomas H. Sharp,[†,‡,¶] Claire L. Williams,[†] Paul M. G. Curmi,[§,‖] Nancy R. Forde,[⊥] Heiner Linke,[⊗]
and Derek N. Woolfson*[,†,‡]

[†]School of Chemistry, University of Bristol, Cantock's Close, Bristol BS8 1TS, U.K.

[‡]School of Biochemistry, University of Bristol, Medical Sciences Building, University Walk, Bristol BS8 1TD, U.K.

[§]School of Physics, University of New South Wales, Sydney, New South Wales 2052, Australia

[‖]Centre for Applied Medical Research, St. Vincent's Hospital, Darlinghurst, New South Wales 2010, Australia

[⊥]Department of Physics, Simon Fraser University, Burnaby, British Columbia V5A 1S6, Canada

[⊗]The Nanometer Structure Consortium (nmC@LU) and Division of Solid State Physics, Lund University, Box 118, 221 00 Lund, Sweden

S *Supporting Information*

ABSTRACT: The design of bioinspired nanostructures and materials of defined size and shape is challenging as it pushes our understanding of biomolecular assembly to its limits. In such endeavors, DNA is the current building block of choice because of its predictable and programmable self-assembly. The use of peptide- and protein-based systems, however, has potential advantages due to their more-varied chemistries, structures and functions, and the prospects for recombinant production through gene synthesis and expression. Here, we present the design and characterization of two complementary peptides programmed to form a parallel heterodimeric coiled

coil, which we use as the building blocks for larger, supramolecular assemblies. To achieve the latter, the two peptides are joined via peptidic linkers of variable lengths to produce a range of assemblies, from flexible fibers of indefinite length, through large colloidal-scale assemblies, down to closed and discrete nanoscale objects of defined stoichiometry. We posit that the different modes of assembly reflect the interplay between steric constraints imposed by short linkers and the bulk of the helices, and entropic factors that favor the formation of many smaller objects as the linker length is increased. This approach, and the resulting linear and proteinogenic polypeptides, represents a new route for constructing complex peptide-based assemblies and biomaterials.
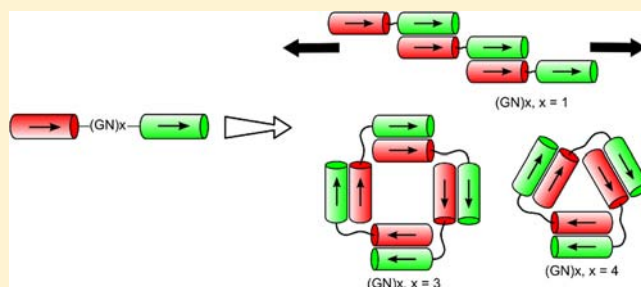
INTRODUCTION

An improved understanding of biomolecular assembly—whether through bioinformatic and theoretical studies, via experimental empiricism, or a combination of both—would have a profound impact in both predictive and synthetic biology.[1,2] That is, if we understood how biological systems are encoded to fold and assemble, we would be able to predict natural biomolecular assemblies from sequence data, to manipulate these predictably and reliably, and to design new biomolecule-based systems *de novo* and with confidence. The power of these links between understanding, prediction and design is evident from the explosion of successful engineering and design studies based on DNA.[3] Straightforward relationships between DNA sequence, strand pairing and structure underpinned the molecular-biology revolution, and they are now fuelling studies to create new DNA-based nanostruc-

tures,[4−6] larger assemblies via DNA origami,[7,8] and even rudimentary molecular motors.[9,10]

Unfortunately, our understanding of sequence-to-structure relationships in polypeptides (i.e., peptides and proteins) is much less mature than that for DNA; in short, we have not yet solved the protein-folding problem. Here, we put to one side the broader aspects of this problem (i.e., those concerning protein-structure prediction) and focus on principles for polypeptide design and engineering. In these respects, with the exception of a small number of cases (for instance, fibrous collagens and zinc fingers)[11−14] there are few direct sequence-to-structure relationships that allow the design of stable polypeptides *de novo*. True, there are several impressive examples of rationally designed peptide self-assembly;[15,16] of

stably folded globular proteins being designed *de novo*;[17] and of the successful manipulation of natural proteins to generate new assemblies, complexes and arrays.[18−20] However, the field is advancing less rapidly than that for DNA-based assembly. Nonetheless, with reliable sequence-to-structure relationships or simply sound principles in place for polypeptide design and engineering, the prospects are considerable. This is for several reasons, most significantly: polypeptides display a large repertoire of stably folded monomer structures and assemblies; in turn, these present scaffolds upon which a rich variety of binding, sensing and catalytic functions can be displayed; and polypeptides can be produced relatively cheaply and in bulk through recombinant expression of synthetic genes. To realize this potential, however, the challenge of designing and engineering polypeptide chains with the same level of predictability and confidence that is possible with DNA needs to be tackled.

One possible solution to this problem of improving protein design and engineering is to take a modular or synthetic-biology approach; that is, to generate peptide- and protein-based parts, or components, and then to learn how to combine and engineer these.[1,21,22] As mentioned above, this has been done and with some success at the whole protein level; for example, Padilla and Yeates,[18] and more recently Sinclair et al.,[19] demonstrate that natural proteins can be used as parts to assemble large objects, and precise arrays by exploiting and combining symmetry axes observed in protein crystal structures. In terms of *de novo* peptide and protein design, the challenge is arguably somewhat harder, as it is not only to combine the parts, but also to generate them in the first place. Some work is underway in this area using modules based on the aforementioned collagen and zinc-finger domains.[23−26] We have advocated the use of a natural protein−protein interaction domain, namely, the α-helical coiled coil.[1,27] As detailed below, this is for several reasons: it is modular, small, and comes in a variety of oligomerization states and topologies; and sequence-to-structure relationships are either available or are being elucidated for many of the more-frequent examples of coiled-coil structures.

The majority of coiled-coil sequences are characterized by the so-called heptad repeat, which is a pattern of hydrophobic (*h*) and polar (*p*) amino acids, *hpphppp*, and often assigned *abcdefg*, with the hydrophobic residues falling at positions *a* and *d*. This provides the first, and simplest, in a series of relationships that link coiled-coil sequence to structure that underpin successful rational designs for these protein domains.[27] When the heptad pattern is displayed on a helical-wheel diagram, it is immediately apparent that the *a* and *d* positions come together on one side of the helix, forming the hydrophobic face of an amphipathic helix, Figure 1A. Two or more such α-helices can associate via these hydrophobic faces to form a structure with a left-handed supercoil.[28,29] Examples of dimeric, trimeric and tetrameric coiled coils are the most common, but higher oligomeric states are also known, and the assemblies can be homomeric or heteromeric, parallel or antiparallel.[29,30] This all gives considerable scope for versatile and widely applicable designs.

Many studies have elucidated sequence determinants for these different oligomer states and topologies, and general 'rules of thumb' for coiled-coil folding and design have been deciphered.[27,31] For example, isoleucine at *a* combined with leucine at *d* tends to specify dimers, isoleucine at both these positions favors trimers, and leucine at *a* paired with isoleucine

Figure 1. Helical-wheel diagrams. (A) These show the positions of the heptad repeat, *abcdefg*, colored by the colors of the rainbow, red−violet, and spun out on a 2D-projection for a parallel dimeric coiled coil. Leaf shapes indicate the direction of the $C_\alpha-C_\beta$ vectors of amino acid residues placed at each position. (B) The sequences for the complementary *de novo* designed peptides DoNA-p1 and DoNA-p2 described herein.

at *d* gives rise to tetrameric coiled coils,[32] although the first of these rules has been reassessed recently.[21] In addition, residues at the *e* and *g* positions are sufficiently close in space to form interhelical electrostatic interactions, which may further stabilize coiled-coil formation and can be used to direct specific coiled-coil heteroassociations,[33−36] and also to direct helix orientation.[37−39] The remaining *b*, *c* and *f* positions are widely considered less influential on coiled-coil oligomer state and partner selection, but for design purposes these are usually kept polar and helix favoring, and they can be used to confer additional functionality to *de novo* peptides.[21,34,40] Using such relationships, specific sequences that form coiled coils of a defined oligomerization state, orientation, and associations can be designed *de novo* with confidence.[27]

Here, we show that a complementary pair of coiled-coil-forming amphipathic α-helical peptides can be joined via disordered flexible peptidic linkers of variable length in order to produce peptidic constructs that self-assemble into various structures, ranging from flexible, micrometer sized fibers, through large colloid-like assemblies, down to discrete nanoscale <10 nm sized objects of defined stoichiometry. In essence, the amphipathic helices associate intermolecularly, and the linker regions determine whether linear or closed assemblies form, Figure 2. Our initial motivation for this was

Figure 2. Strategy and proposed assemblies for the designed helix-linker-helix constructs described. A schematic detailing the proposed assembly of the *de novo* designed peptidic constructs: (A) the construct consists of two complementary coiled-coil-forming peptides (green and red cylinders), joined by a disordered peptidic linking region (black lines). (B) The sequences of the coiled coils are such that antiparallel assembly (shown by the arrows pointing from the N- to C-termini) is disfavored. Whereas, intermolecular, parallel, heterodimeric assembly is promoted leading to the possibility of fibrous structures when short linkers are employed (C); closed, discrete structures when longer linking regions are used (E); and more-complex aggregates at intermediate loop lengths (D). The black arrows in (C) indicate that the fibrous assemblies can propagate in two directions.

to complete a design cycle and realize a peptide-based hub for the assembly of a *de novo* protein-based motor.[35,41] However, we believe that the design principles and strategy, and the structures produced may have broader potential and applications.

MATERIALS AND METHODS

Peptide Synthesis and Purification. All peptides were synthesized on a Liberty CEM microwave synthesizer using standard Fmoc chemistry, rink-amide resin and HBTU activation. Peptides were N-terminally acetylated and C-terminally amidated. They were purified by reversed-phase HPLC using a Vydac C18 column, and their identities confirmed by MALDI-TOF mass spectrometry using an α-cyano-4-hydroxycinnamic acid (CHCA) matrix.

Disulfide Exchange. N- and C-terminally Cys labeled analogues of the two, 3-heptad peptides were synthesized. The sequences were designed to match as closely with the parents as possible, while giving each peptide and disulfide-bonded combination a unique mass, Table 1. Samples for disulfide-exchange experiments were prepared with 20

Table 1. The Sequences of DoNA-p1 and DoNA-p2, along with the N- and C-Terminal Cysteine Derivatives

Peptide	Sequence
	def gabcdef gabcdef gabcdef ga
DoNA-p1	EIKALEQ EIAALKQ KIAWLKQ
DoNA-p1N	CGG EIKALEQ EIAALKQ KIAWLKQ
DoNA-p1C	QG EIKALEQ EIAALKQ KIAWLKQ GC
DoNA-p2	KIKALKQ EIAALKQ EIAYLEQ
DoNA-p2N	CGG KIKALKQ EIAALKQ EIAYLEQ
DoNA-p2C	KIKALKQ EIAALKQ EIAYLEQ GC

μM of each peptide in phosphate-buffered saline (PBS, pH 7.4), 4 mM oxidized glutathione and 1 mM reduced glutathione in the presence or absence of 6 M guanidine HCl. Samples were left to equilibrate at 20 °C. Peaks were identified by reversed-phase HPLC and the identities of the peaks confirmed by MALDI-TOF mass spectrometry.

Circular Dichroism Spectroscopy. Measurements were made with a JASCO-J815 spectropolarimeter fitted with a Peltier temperature controller. Peptide solutions were made in PBS (pH 7.4) and examined in either 1 or 2 mm cuvettes containing a total of 200 or 400 μL of peptide solution, respectively. Spectra were recorded at 5 °C using a 1 nm interval, 1 nm bandwidth and a 2 s response time. Ellipticities (in mdeg) were baseline corrected and converted to molar ellipticities (deg cm^2 dmol·res^{-1}) by normalizing for the concentration of peptide bonds and for the path length of the cell. Theoretical spectra were calculated by taking into account the number of residues in both the helices (42 residues) and the linking regions (2−10 residues), for example, MRE(DoNA-GN$_1$, theoretical) = (42/(42 + 2)) × MRE(DoNA-p1:DoNA-p2 heterodimer, experimental). Thermal unfolding data were recorded by following the signal at 222 nm through 1 °C min^{-1} ramps using a 1 nm bandwidth. Where appropriate, the midpoints (T_m) of the curves were determined by taking the second derivatives of the melting curves.

Size Exclusion Chromatography. Experiments were performed using a Superdex 75 10/30 GL column (nominal molecular-weight range: 3−70 kDa). Samples were prepared at 200 μM peptide concentration in PBS (pH 7.4). Chromatograms were run over 60 min with a flow rate of 0.5 mL min^{-1}, using PBS (pH 7.4) as the eluent. A 3-heptad dimeric coiled coil was used as the sizing standard and eluted at 32 min.

Dynamic Light Scattering. Measurements were made using a Malvern Zetasizer Nanoseries instrument. Samples were prepared at 100 μM peptide concentration in PBS (pH 7.4). Samples were

centrifuged prior to analysis to remove any large particulate material. Measurements were made at 20 °C using automated settings. The data were analyzed using the associated DTS Nano particle-sizing software. Predictions for the hydrodynamic diameters were obtained using *Hydropro*.[42] Coiled-coil atomic coordinate files were produced using the MAKECCSC program.[43]

Analytical Ultracentrifugation. Sedimentation-equilibrium experiments were conducted at 20 °C in a Beckman-Optima XL-I analytical ultracentrifuge using an An-60 Ti rotor. Solutions were prepared in PBS (pH 7.4) with peptide concentrations in the range 75−400 μM and spun at speeds in the range 20 000−50 000 rpm. Data sets were fitted initially to single, ideal species models using *Ultrascan*.[44] DoNA-p2 was subsequently fitted to a model for a monomer−dimer equilibrium. The partial specific volume for each of the various peptides and the solvent density was calculated using *Sednterp*.[45]

Transmission Electron Microscopy. Samples were prepared at 10 and 100 μM peptide concentrations, spotted onto carbon and Formvar-coated copper grids and left for 1 min. After wicking away any excess liquid, the grids were washed three times with deionized water. Uranyl acetate was used to negatively stain the samples for 1 min and then it was wicked off. After drying for 10 min, the grids were inserted into a Tecnai T12 electron microscope (FEI Company, The Netherlands) and imaged at 120 kV. Images were captured on an Eagle 4k × 4k CCD camera (FEI Company, The Netherlands).

Selection of Linker Sequences. A set of nonredundant (≤70% sequence identity at the coiled-coil level) sequential antiparallel coiled coils were extracted from the CC+ database.[46] A total of 460 antiparallel coiled coils were identified, each comprising two helices adjacent to one another in the protein sequence and without any other intervening secondary structural elements. The sequences of loop regions of ≤5 residues long were extracted. In this way, 151 loops were identified, aligned and analyzed using Weblogo[47] to identify which residues would be most suitable at each position in the linker sequence.

Model Building. A model of the coiled coil formed by two peptides DoNA-p1 and DoNA-p2 was built using standard homology modeling methods and based on the GCN4 leucine-zipper structure (PDB identifier, 2ZTA). Two copies of this model were joined between the C-terminus of one DoNA-p1 peptide in the first model to the N-terminus of one DoNA-p2 peptide in the second model, via a linker of (GN)$_n$ repeats where n = 0−5 (DoNA-p1.GN$_n$.DoNA-p2), in a helical conformation. This yielded six all-helical termolecular complexes, corresponding to two sides and one linker of the respective oligomeric states of these peptide sequences, as starting points for molecular-dynamics simulations. The oligomeric structures, namely, the DoNA-GN$_4$ trimer and DoNA-GN$_3$ tetramer, were constructed in a similar fashion, except that the coiled-coil segments were juxtaposed appropriately using molecular graphics, and the linker regions built using the loop building tools in InsightII (Accelrys).

Simulations. Each model was set up for simulation in the following manner using the GROMACS 4.5.3 suite of tools. First, hydrogen atoms were added using pdb 2gmx, and consistent with pH 7; the AMBER03 forcefield and TIP3P water model were chosen. Next, a dodecahedral periodic-boundary box defined such that the distance between any atom in the complex and the box boundary was ≥1.5 nm (editconf). This box was filled with water molecules (genbox) and sodium chloride ions to give neutral overall charge and a salt concentration of 0.15 M (genion). The system was energy minimized and subjected to 0.2 ns of molecular dynamics at 298 K as an NPT ensemble under PME periodic boundary conditions, while restraining the peptide atoms to their initial positions. This procedure acted as an initial relaxation and equilibration step. The restraints were removed and the molecular-dynamics simulation continued for a further 100 ns, saving structures at 0.1 ns intervals for analysis. These simulations proceeded at a rate of 6−10 ns per day using 32 cores of the Bristol HPC BlueCrystal (phase 2). Hence, the complete set of simulations required approximately 100 000 CPU hours.

Simulation Analysis. The trajectories were processed (trjconv) to remove PBC effects and solvent and inspected using VMD.[48]

15459

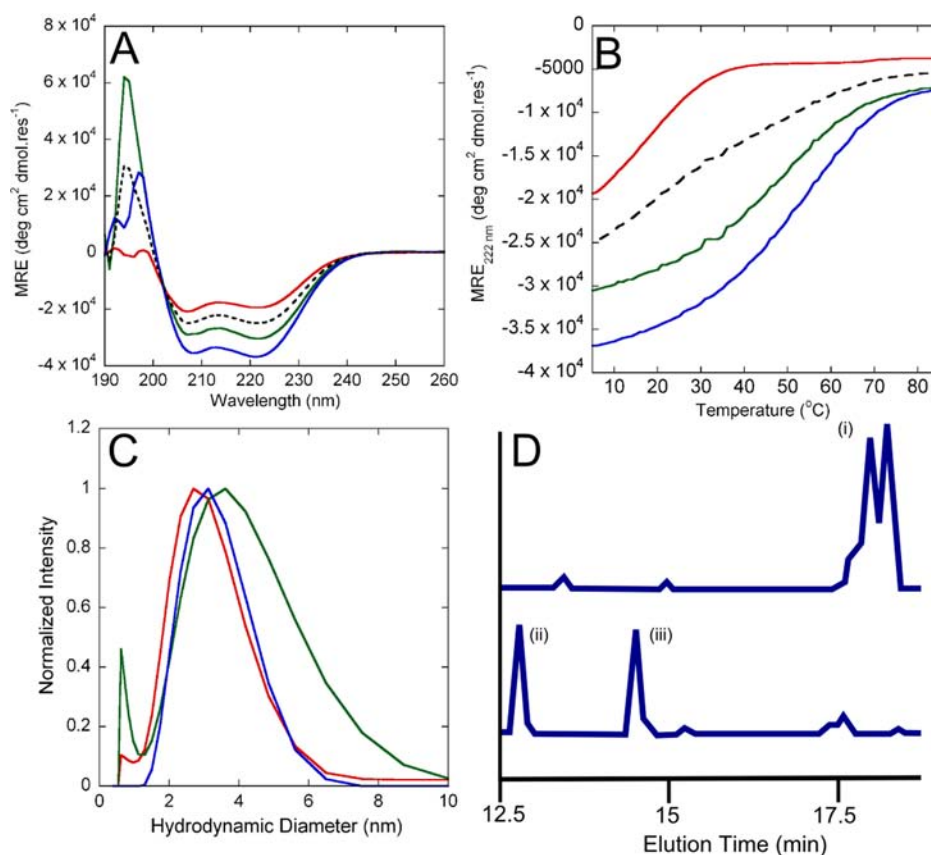dx.doi.org/10.1021/ja3053943 | *J. Am. Chem. Soc.* 2012, 134, 15457−15467

Figure 3. Characterization of the designed peptides DoNA-p1 and DoNA-p2. (A) CD spectra at 5 °C for DoNA-p1, DoNA-p2, the 1:1 mixture of the two peptides and the theoretical average of the mixture. (B) Thermally induced unfolding curves for the peptides. (C) Dynamic light scattering (DLS) data for the individual peptides, the smaller peaks observed at approximately 0.7 nm for both DoNA-p1 and DoNA-p2 are attributed to peptide monomers. Key: DoNA-p1, green; DoNA-p2, red; theoretical average, dashed black line; 1:1 mixture, blue. Conditions: 100 μM peptide concentration in phosphate buffered saline (PBS; 10 mM phosphate, 137 mM NaCl, 2.7 mM KCl, pH 7.4). (D) Truncated analytical HPLC traces from the disulfide-exchange experiments conducted with the Cys-tagged DoNA-p1 and DoNA-p2 peptides. The uppermost is for the four Cys-tagged peptides mixed under denaturing conditions (6 M guanidine hydrochloride). The group of peaks (i) corresponds to each of the four peptides bonded to glutathione. The lowermost is that for the same peptides mixed under native conditions. Peak (ii) corresponds to the parallel heterodimer formed by the N-terminally tagged peptides, and peak (iii) to the disulfide-bonded parallel heterodimer formed by the C-terminally tagged peptides. The full traces are shown in Figure S3.

Structures were also exported as PDB files every 10 ns for figure generation (trjconv). The angles between the coiled coils on either side of the linker region, in the noncyclic models, were estimated as follows. First two vectors were defined between C_α atoms in the long peptide, one between residues Gln-7 and Gln-14 in all cases, and the second between residues Gln-(28 + 2n) and Gln-(35 + 2n) for models DoNA-p1.GN$_n$.DoNA-p2. These vectors were passed to the analysis tool (g_sgangle) via an index file that produced the angle trajectories.

■ RESULTS

Designing a Parallel Heterodimeric Coiled-Coil Peptide Building Block. To generate the self-assembling constructs, we required two straightforward, self-assembling peptides, plus a set of flexible linkers of variable length. For the former, we opted to design *de novo* a parallel coiled-coil heterodimer, that is, a complementary pair of coiled-coil forming peptides. As illustrated in Figure 1B, the sequences of these peptides were based on canonical heptad sequence repeats (*abcdefg*), with isoleucine placed at the *a* positions and leucine at *d* in order to form the hydrophobic core and to help direct dimer formation.[21,32] Glutamic acid and lysine residues were placed at the *e* and *g* positions to promote interhelical salt-bridge interactions. These were patterned to maximize the number of salt bridges formed in the parallel heterodimer

orientation, and to disfavor alternatives such as the antiparallel heterodimer and any homodimer orientation. The *b, c,* and *f* positions were filled with alanine and glutamine to maximize helicity, with the exception of one *b* position, which was set to lysine to aid solubility, and a single *c* position, which was made either tyrosine or tryptophan to facilitate spectroscopic characterization.

The peptides were made 3 heptads long to ensure folding in the micromolar (μM) peptide-concentration range.[49] Note, we chose not to use an asparagine residue at an *a* site as, while this does help specify dimer,[21,50] it destabilizes coiled-coil assemblies and we wanted to keep these component peptides as short as possible to allow the later experiments described below; in addition, we reasoned that specifying obligate heterodimers in itself would also help direct dimer assembly rather than higher-order structures. In addition to the two parent peptides, which were dubbed DoNA-p1 and DoNA-p2, for Donut-shaped Nano-scale Assembly, N- and C-terminal cysteine derivatives, were synthesized to facilitate disulfide-exchange experiments to test the proposed helix partnering and orientation. The full sequences for all of the resulting peptides are given in Table 1.

Characterization of the Coiled-Coil Peptide Building Blocks. The coiled-coil-forming peptides (DoNA-p1 and DoNA-p2) were synthesized and characterized in solution using a combination of circular dichroism (CD) spectroscopy, dynamic light scattering (DLS), analytical ultracentrifugation (AUC) and disulfide cross-linking experiments.

CD spectroscopy revealed that both DoNA-p1 and DoNA-p2 were partially folded at 100 μM peptide concentration in phosphate buffered saline (PBS) at 5 °C, with DoNA-p1 being more folded (80% helical) than DoNA-p2 (53% helical), Figure 3A. However, when mixed in equimolar amounts, the resulting spectrum was more helical (97%) than the spectra for either of the individual peptides, and also for the average of the two isolated spectra, Figure 3A. This indicated that the two peptides interacted to form a heteromeric helical structure. Similarly, when the stabilities of the peptides were investigated via thermally induced unfolding monitored by the CD signal at 222 nm, the 1:1 mixture of the two peptides was more stable than either of the individual peptides, Figure 3B, with a T_m of 54 °C; while DoNA-p1 had a T_m of 49 °C and an accurate T_m could not be obtained for DoNA-p2 as it was only partially folded at 5 °C.

Similar behavior was observed when the peptides were analyzed at the lower concentrations of 10 and 1 μM, although the helicities and stabilities were all reduced, consistent with concentration-dependent assembly of higher-order structures, Figure S1.

Initially, dynamic light scattering (DLS) was used to probe the sizes of the species formed in solution. For all three samples (DoNA-p1, DoNA-p2, and the 1:1 mixture), the DLS traces were dominated by a peak centered on a hydrodynamic diameter of 3 nm, Figure 3C; the observed diameters of DoNA-p1 and DoNA-p2 were distinct at 3.6 and 2.7 nm, respectively, whereas a peak for the mixture was observed at 3.1 nm. These data are consistent with the formation of three-heptad dimeric coiled coils; Hydropro predicted the hydrodynamic diameter of a three-heptad coiled-coil model to be ~3.2 nm.[42]

Analytical ultracentrifugation (AUC) was used to test the oligomeric state of the species formed by the individual peptides and the 1:1 mixture, Figure S2. This showed that DoNA-p1 formed a dimer in solution, with a molecular weight returned from fits assuming a single ideal species of 5118 Da (95% confidence limits: +22 Da, −53 Da), compared with the monomer mass of 2493 Da; the data for DoNA-p2 fitted well to a monomer−dimer equilibrium model with a dissociation constant of 125 μM, consistent with the partial folding of ~50% at 100 μM concentration observed by CD spectroscopy; and those for the mixture fitted as a single ideal species of molecular weight 5053 Da, (95% confidence limits: +21 Da, −18 Da), compared with the calculated heterodimer molecular mass of 4963 Da.

Finally, to determine the orientation of the DoNA-p1:DoNA-p2 heterodimer, disulfide-exchange experiments were performed in the presence and absence of 6 M guanidinium chloride as a denaturant. All four of the cysteine-tagged peptides were mixed in a glutathione-based redox buffer, left to equilibrate at room temperature for one week, and then analyzed by HPLC and MALDI-TOF mass spectrometry. Under denaturing conditions, only glutathione adducts were observed, whereas under folding conditions, only two species were observed, Figures 3D and S3, and both were identified as parallel heterodimers. This should be compared with the 10 possible disulfide-linked dimers from all combinations of the four cysteine-terminated peptides in the absence of specific parallel heterodimer interactions.

In summary, peptides DoNA-p1 and DoNA-p2 combine to form a stable, concentration dependent, parallel, α-helical heterodimer consistent with our coiled-coil design. With these peptides in hand, we moved on to linking them to form self-assembling constructs.

Identifying Sequences To Link DoNA-p1 and DoNA-p2. To generate the full-length, self-assembling constructs, the two designed peptides needed to be joined by linkers. Ideally, these would be disordered, modular and chemically accessible. To guide this choice, we conducted a bioinformatics analysis of loop regions separating antiparallel coiled coils, that is, helix-turn-helix structures, in the CC+ database.[46] The most common dipeptide repeat unit found, glycine−aspartic acid, was not used due to concerns over aspartimide formation during peptide synthesis.[51] Instead, we used the next most frequent dipeptide, glycine−asparagine (GN) as the basis for our linkers, Figure S4. A series of constructs incorporating increasing numbers of the GN units was designed and synthesized, Table 2.

Table 2. Amino Acid Sequences of the Series of the Self-Assembling GN-Linked Constructs[a]

Peptide	Sequence						
	gabcdef	*gabcdef*	*gabcdef*	----------	*gabcdef*	*gabcdef*	*gabcdef*
DoNA-GN$_1$	EIAALEQ	EIAALKQ	KIAALKQ	----GN----	KIKALKQ	EIAALKQ	EIAYLEQ
DoNA-GN$_2$	EIAALEQ	EIAALKQ	KIAALKQ	---GNGN---	KIKALKQ	EIAALKQ	EIAYLEQ
DoNA-GN$_3$	EIAALEQ	EIAALKQ	KIAALKQ	--GNGNGN--	KIKALKQ	EIAALKQ	EIAYLEQ
DoNA-GN$_4$	EIAALEQ	EIAALKQ	KIAALKQ	-GNGNGNGN-	KIKALKQ	EIAALKQ	EIAYLEQ
DoNA-GN$_5$	EIAALEQ	EIAALKQ	KIAALKQ	GNGNGNGNGN	KIKALKQ	EIAALKQ	EIAYLEQ

[a]The color scheme is based on the order of colors in visible spectrum (omitting yellow as it has poor contrast in figures) and is used throughout this manuscript; i.e, DoNA-GN$_1$, red; DoNA-GN$_2$, orange; DoNA-GN$_3$, green; DoNA-GN$_4$, blue; and DoNA-GN$_5$, violet. All peptides were N-terminally acetylated and C-terminally amidated during synthesis.

Solution-Phase Characterization of the GN-Linked Constructs. Concentration dependent CD spectroscopy confirmed that all of the GN-linked constructs were predominantly α-helical at both 10 μM, Figure 4A, and 100 μM peptide concentrations, Figure S5. The helicities of the peptides decreased with increasing linker length, consistent with our aim that the GN linkers should be largely unfolded. However, over and above this expected loss in CD intensity, we observed lower helicities compared with the theoretical spectra calculated assuming the helicity of the DoNA-p1:DoNA-p2 mixture and the proportion of these sequences in each GN-linked construct, Table 3.

At 10 μM peptide concentration, the shapes of the thermal unfolding curves for the GN-linked constructs varied, Figure 4B. The curve for DoNA-GN$_1$ was not a simple sigmoid, indicating complex, non-two-state unfolding behavior. The unfolding curves for DoNA-GN$_{2−5}$ however, although broad, appeared sigmoidal and T_m's were determined for these transitions, Figure 4B and Table 3. The curves recorded for 100 μM samples were even more complex for DoNA-GN$_1$ and also for DoNA-GN$_2$. However, generally the lower-temperature CD signals were more intense than those recorded at 10 μM
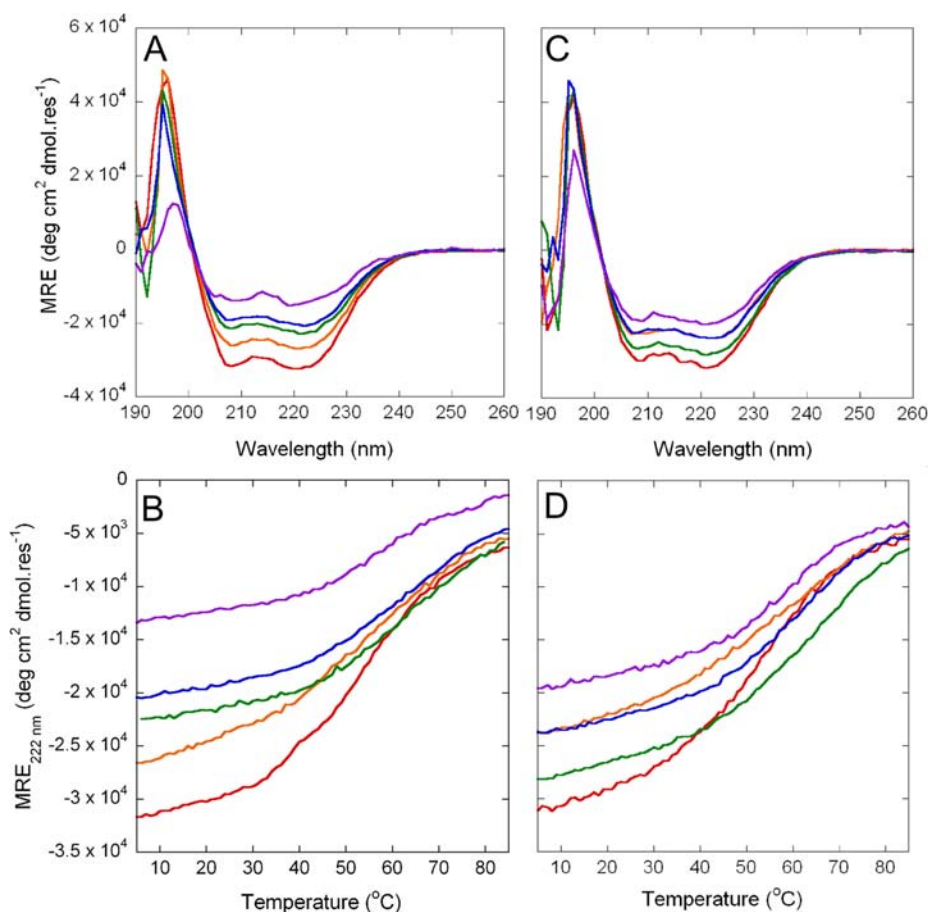
Figure 4. CD spectra and thermal-unfolding curves for nonannealed and annealed samples of the GN-linked constructs. (A) CD spectra at 5 °C, 10 μM peptide concentration in PBS, for nonannealed peptide samples. (B) Thermal-unfolding curves monitored at $[\theta]_{222}$ for the nonannealed peptide samples at 10 μM peptide concentration. (C) CD spectra at 5 °C, 10 μM peptide concentration for annealed peptide samples. (D) Thermal unfolding curves monitored at $[\theta]_{222}$ for the annealed peptide samples at 10 μM peptide concentration. Key: DoNA-GN$_1$, red; DoNA-GN$_2$, orange; DoNA-GN$_3$, green; DoNA-GN$_4$, blue; and DoNA-GN$_5$, violet.

Table 3. Details of the Mean Residue Ellipticity (MRE; deg cm^2 dmol·res^{-1}) and Percent Helicity (Values in Parentheses for Columns 3 and 4) at 5 °C, and T_m Values for Nonannealed and Annealed DoNA-GN Peptides at 10 μM Peptide Concentration

Peptide	MRE$_{222}$ Theoretical	MRE$_{222}$ Nonannealed	MRE$_{222}$ Annealed	Nonannealed T_M (°C)	Annealed T_M (°C)
DoNA-GN$_1$	−31,194	−31,777 (101)	−31,439 (101)	N/A	55
DoNA-GN$_2$	−29,762	−26,453 (89)	−23,807 (80)	60	58
DoNA-GN$_3$	−28,522	−22,578 (79)	−27,825 (96)	65	67
DoNA-GN$_4$	−27,380	−20,689 (76)	−23,699 (87)	63	63
DoNA-GN$_5$	−26,328	−14,394 (55)	−19,701 (75)	58	60

peptide, and in all cases, the stabilities were too high to obtain T_m values, Figure S5.

Interestingly, some of the constructs, particularly DoNA-GN$_{3-5}$, were more helical after heat denaturation and cooling back to 5 °C than when freshly mixed. To investigate this further, peptide samples were annealed by heating to 90 °C for 10 min, and then cooling back to 20 °C at a rate of 1 °C min^{-1} prior to recording further CD data. Subsequent CD spectra collected at 5 °C indicated that peptides DoNA-GN$_{3-5}$ were

more helical, Figure 4C, Table 3; the helicity of DoNA-GN$_1$ was not altered; and that for DoNA-GN$_2$ decreased slightly. The effects of annealing on the thermal-unfolding transitions were that all peptides, DoNA-GN$_{1-5}$, gave sigmoidal curves, Figure 4D, at least at 10 μM peptide concentrations, allowing T_m values to be calculated for all constructs, Figure 4D, Table 3. However, these did not change significantly or consistently as did the MRE$_{222}$ values, for DoNA-GN$_{3-5}$ at least. Again, complete unfolding transitions were not observed at 100 μM peptide concentration, and for DoNA-GN$_1$, the transition remained complex, Figure S5.

By linking two coiled-coil peptides together, it is possible that stable, cooperatively folded units arise simply through intra-molecular helix-turn-helix structures.[39] However, the concentration-dependent and somewhat complex thermal-unfolding behavior of the GN series indicated that this was not the case. Therefore, we probed the assemblies by dynamic light scattering (DLS). This was done for both nonannealed and annealed samples to investigate whether annealing affected the size of any assemblies formed. For DoNA-GN$_1$ and DoNA-GN$_2$, two species were observed with both samples: for the nonannealed samples, assemblies with hydrodynamic diameters of approximately 8−10 nm, Figure 5A, plus much broader peaks at approximately 100 nm, Figure 5B. After annealing, the peaks at both diameters were sharper, Figure 5C,D. For nonannealed samples of the DoNA-GN$_{3-5}$ constructs, only the
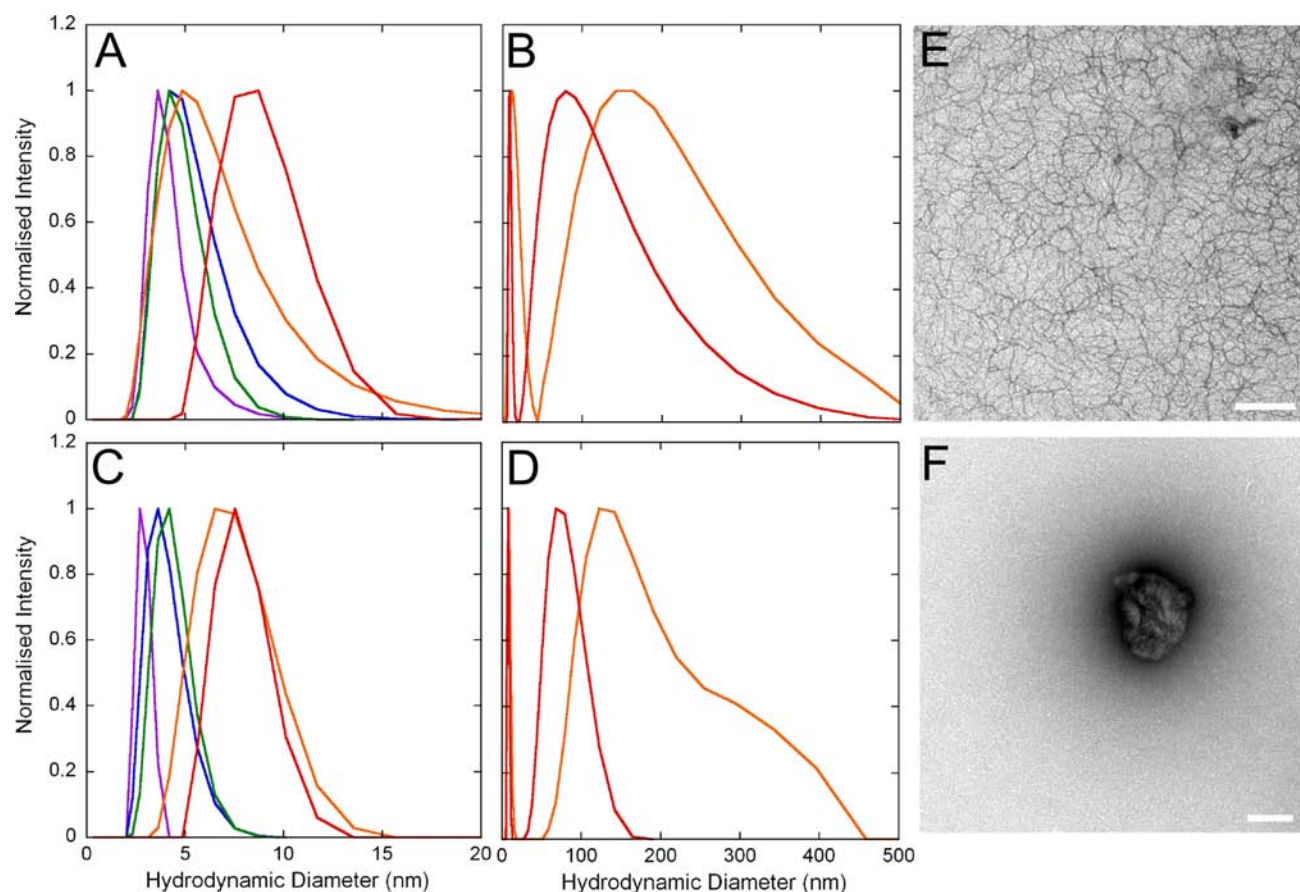
Figure 5. Large assemblies formed by DoNA-GN constructs probed by DLS and TEM. (A) DLS data for nonannealed peptide samples. (B) Expanded DLS data for nonannealed samples of DoNA-GN$_1$ and DoNA-GN$_2$, illustrating the presence of larger self-assembled species. (C) DLS data for annealed peptide samples. (D) Expanded DLS data for annealed peptide samples of DoNA-GN$_1$ and DoNA-GN$_2$, again illustrating the presence of a second, larger species. (E) TEM micrograph of fibers formed by annealed samples of DoNA-GN$_1$. (F) TEM micrograph of the large assemblies formed by annealed samples of DoNA-GN$_2$. Key: DoNA-GN$_1$, red; DoNA-GN$_2$, orange; DoNA-GN$_3$, green; DoNA-GN$_4$, blue; and DoNA-GN$_5$, violet. Conditions: 100 μM peptide concentration in PBS, pH 7.4, 20 °C. The scale bars for the images in panels (E) and (F) are 100 nm.

smaller species were observed, with hydrodynamic diameters in the range 3−5 nm, Figure 5A; and, again, annealing narrowed the size distribution, Figure 5C. Annealing also decreased the average size of assemblies formed for all constructs except for DoNA-GN$_2$, where the hydrodynamic diameter of the smaller-diameter peak increased, compare Figure 5A,C, and a proportion of the very large (200−400 nm) species remained.

To gain further insight as to the assemblies formed by DoNA-GN$_{3−5}$, size-exclusion chromatography (SEC) was performed, Figure S6. For the nonannealed samples, a major peak eluted after 25 min for both DoNA-GN$_3$ and DoNA-GN$_4$ and after 27 min for DoNA-GN$_5$. Both nonannealed samples of DoNA-GN$_3$ and DoNA-GN$_4$ had several other, smaller peaks that eluted between 30 and 40 min, similar to control coiled-coil dimers. Annealed samples of both these peptides revealed the presence of the major peak only, which was narrower than for the nonannealed samples. For DoNA-GN$_5$, there was little difference between the traces for the nonannealed and annealed samples.
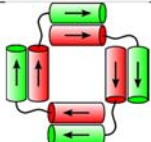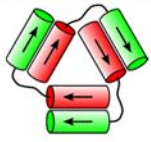
Analytical Ultracentrifugation of the GN-Linked Constructs. Sedimentation-equilibrium experiments were performed using analytical ultracentrifugation (AUC) to probe further the assemblies of the GN-linked peptides. For each construct, both nonannealed and annealed samples were prepared and analyzed, Figure S7. For DoNA-GN$_1$ and DoNA-

GN$_2$, the majority of each sample sedimented completely while setting up the experiments, that is, spinning at 3000 rpm, and detailed analyses were not possible. This is consistent with the DLS, and indicates further that these peptides formed large, ≥MDa-sized objects.

To determine how much peptide was incorporated into these larger assemblies, samples were centrifuged, to remove such aggregates, and the concentrations of peptide in the supernatants determined; the supernatant should contain only peptides assembled as small species. We found that for DoNA-GN$_1$, 80% of the nonannealed and 85% of the annealed peptide was incorporated into the larger assemblies, and for DoNA-GN$_2$, 72% of the nonannealed and 74% of the annealed peptide sample formed larger assemblies.

For nonannealed samples of DoNA-GN$_{3−5}$, the AUC experiments indicated much smaller assemblies. However, they also implied that various species were formed, as noninteger numbers of peptides were returned from the curve-fitting analyses of the data. For example, for DoNA-GN$_{3−5}$ weights of 4.5×, 3.7×, and 2.5×, the monomer masses were returned from fits assuming single, ideal species, Table 4. These could have been indicating monomer−multimer equilibria, but attempts to analyze the data sets with more-complex models did not improve the fits.

Table 4. Solution-Phase Molecular Weights Determined by AUC for the DoNA-GN$_3$–DoNA-GN$_5$ Constructs for Both the Nonannealed and Annealed Samples, along with Accompanying Schematics for the Proposed Assemblies

Peptide	Monomer Molecular Mass (Da)	Weight by AUC (Da) Nonannealed	Weight by AUC (Da) Annealed	Proposed Assembly Annealed
DoNA-GN$_1$	4902.8	N/A – forms fibers	N/A – forms fibers	Fibrous
DoNA-GN$_2$	5074	N/A – forms large assemblies	N/A – forms large assemblies	Colloid-sized assemblies
DoNA-GN$_3$	5245.1	23,500	20,500	
DoNA-GN$_4$	5416.3	20,000	15,800	
DoNA-GN$_5$	5587.4	13,900	14,000	

By contrast, analyses of the AUC data for the annealed samples of DoNA-GN$_3$ and DoNA-GN$_4$ did reveal species of defined sizes; the weights returned from fits assuming single, ideal species were for tetramer and trimer, respectively. These molecular weights were smaller than those returned from the fits to the data from the nonannealed samples, again consistent with the DLS, Table 4.

For DoNA-GN$_5$, however, there was little difference in the molecular weights returned for the nonannealed and annealed samples with either simple- or complex-fitting models. This suggests that the peptide forms both dimers and trimers in solution.

Electron Microscopy of the DoNA-GN$_1$ and DoNA-GN$_2$ Constructs. As the DLS and AUC analyses indicated that DoNA-GN$_1$ and DoNA-GN$_2$ formed large structures, these assemblies were examined by negative-stain transmission electron microscopy (TEM). Again, both nonannealed and annealed samples at 10 and 100 μM peptide concentrations were investigated due to the different behaviors observed under these conditions. At both concentrations, DoNA-GN$_1$ formed short, thin, flexible fibers, Figures 5E and S8. The fibers formed from the nonannealed samples gave typical negatively stained images, Figure S8, whereas those prepared from annealed samples stained positively suggesting that they were actively taking up stain, Figure 5E. Annealing appeared to produce thickened fibers at the higher peptide concentration of DoNA-GN$_1$. Both of these effects have been observed before with sticky end-assembled peptide fibers.[52,53] Because of the different modes of staining, however, it was difficult to quantitate the widths accurately, although measurements were taken and do corroborate this assertion, Figure S9.

Interestingly, and in contrast to DoNA-GN$_1$, the non-annealed and annealed samples of DoNA-GN$_2$, at either concentration, revealed rounded particles with diameters of approximately 100 nm, Figures 5F and S8. These particles did not appear to have any regular internal structure, and it was not possible to distinguish whether these were ring-like, spherical, or some other type of aggregate.

The sizes of these assemblies formed by DoNA-GN$_2$ and observed by TEM, correlate with the sizes implied by DLS for the large assemblies. However, as DoNA-GN$_1$ forms fibers, and not spherical objects, that the DLS and TEM data do not correlate well is not surprising: to determine hydrodynamic diameters of particles by DLS requires that they are treated as globular; long, thin fibers have very different diffusion properties and the hydrodynamic "diameters" reported are not meaningful.

Modeling DoNA-GN$_3$ and DoNA-GN$_4$. On the basis of the AUC results, we modeled the DoNA-GN$_3$ and DoNA-GN$_4$ constructs as cyclic assemblies of DoNA-p1-turn-DoNA-p2 structures, Figures 6A,B. Molecular dynamics simulations of these models were performed to probe whether these proposed conformations were stable at least *in silico*. The DoNA-GN$_3$ construct changed conformation after approximately 60 ns into a 'diamond shape', as opposed to the starting 'square shape', Figure 6C. This simulation was run for another 100 ns (200 ns total) but no further change in the conformation occurred, Figure S10. Despite this change, which reduced the size of the central cavity, the proposed tetrameric assembly remained stable for the duration of the simulation. Likewise, the model for the trimeric DoNA-GN$_4$ construct was stable over the 100 ns simulation. Some contraction in the central cavity of the structure was observed, largely due to the rotation of two of the coiled coils into the plane of the triangular structure, Figure 6D, but otherwise the overall shape remained unchanged, Figure S10.

We also modeled the turn regions for all constructs to explore how much flexibility each linker could afford, Figure S11. The starting models for the simulations were the corresponding DoNA-GN$_{0-5}$ peptides in fully helical con-
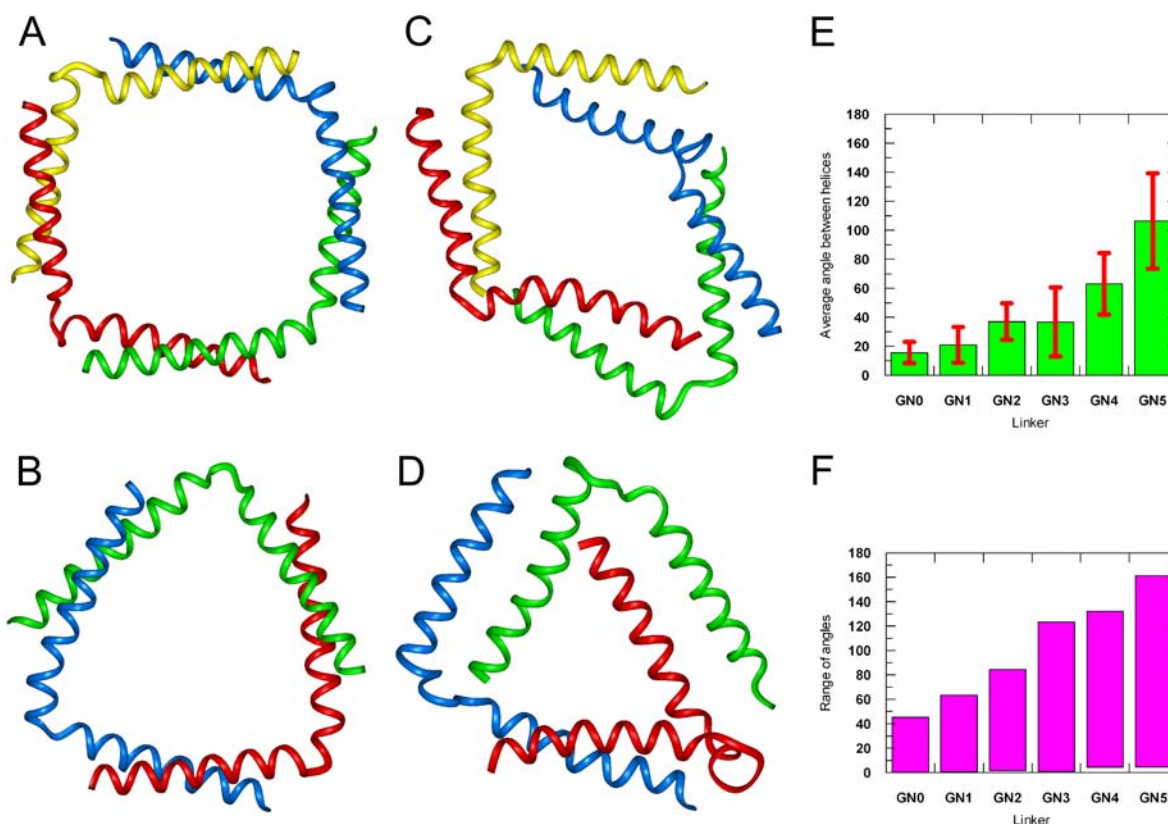
Figure 6. Molecular dynamics simulations for DoNA-GN$_3$ and DoNA-GN$_4$, and the linker regions. Models were built for both the DoNA-GN$_3$ (A) and DoNA-GN$_4$ (B) constructs. Molecular dynamics simulations were performed on these models to investigate their conformational behavior, and structures at 0 ns (A and B) and 100 ns (C and D) are shown. DoNA-GN$_3$ appeared to form a 'diamond shaped' assembly (C), while DoNA-GN$_4$ remained triangular in shape (D). Models of the linking regions underwent similar simulations and the results were analyzed to show the average (E) and extent (F) of the bend angle produced by the different linkers during the simulations (error bars in panel (E) represent the standard deviations).

formations, each bound to a copy of peptides DoNA-p1 and DoNA-p2 giving a series of ternary complexes comprising two coiled coils separated by the linker. Molecular dynamics simulations were run for 100 ns for each model. The trajectories were analyzed by measuring the angle between the major axes of the coiled coils in each model. The starting and representative structures visited during the simulations are shown in Figure S11. The results are in good agreement with the experimental data, the amount of flexibility afforded by the linker is increased with increasing linker length, with those in DoNA-GN$_3$ and DoNA-GN$_4$ able to adopt the 90° and 120° angles required for the closed structures that we propose are formed, Figure 6E&F.

■ DISCUSSION AND CONCLUSION

We have presented a protein-design experiment in which two peptide components (a parallel, α-helical coiled-coil hetero-dimer, comprising DoNA-p1 and DoNA-p2; and flexible, peptidic linkers) are combined to generate a series of DoNA-p1-linker-DoNA-p2 polypeptides. These constructs self-assemble via DoNA-p1:DoNA-p2 interactions to give a range of materials and objects that span fibers on the micrometer scale; through large ring-like, spherical or aggregated particles with colloid-like dimensions of ~100 nm; down to discrete nanoscale objects with dimensions of a few nanometers. The designs have been probed extensively and verified using a combination of spectroscopy, size exclusion chromatography, light scattering, centrifugation and microscopy techniques. In addition, for the smaller assemblies, molecular modeling and

dynamics have been used to explore the feasibility and conformational flexibilities of the proposed structures.

An intriguing observation from constructing and characterizing this self-assembling peptide system is that as the linker length between the helices is increased, the size of the resulting assemblies is reduced. Although this was our aim at the start of the experiment, we had not envisaged the breadth of assemblies that we would encounter. We propose that this results from a balance between entropic and steric considerations around the linker region as follows.

First, all of the assemblies are driven by the heteropairing of DoNA-p1 and DoNA-p2. Thus, in the case where the two helices are separated by a sufficiently long and flexible linker, we would expect a folded monomer, at least at high dilution, that is, DoNA-p1 and DoNA-p2 could interact intramolecularly. Clearly, with the current linkers, we have not reached this limit. Because DoNA-p1 and DoNA-p2 are designed to interact with a parallel register, we estimate that linkers of the order of 20 residues or more in length would be required to achieve this. (Note, two-helix constructs with such linker lengths were beyond the limits of peptide chemistry used in this study.) Thus, for the series described here (with linkers in the range 2–10 residues), the DoNA-p1−DoNA-p2 interactions are restricted to being intermolecular. In this case, for fully flexible linkers, and without any other steric constraints, entropy should drive the system to form the maximum number of the smallest-sized particles. However, as there are steric constraints (both in terms of the helix−helix angles the linkers allow, and because the helices have bulk and will reduce the volume available to be

explored), the assemblies observed will depend on linker length in some complex way. Therefore, the best way to explore this relationship is through empirical experimentation as performed here. Nonetheless, we have begun to examine these constraints through molecular dynamics, and the flexibilities afforded by 6- to 10-residue linkers appear compatible with the formation of discrete objects that we observe which include tetramers and trimers of the constructs.

At the other end of the linker lengths (i.e., a 2-residue linker), the steric constraints of linker inflexibility and helix bulk win out, and this construct essentially acts as a rigid rod, which leads to fiber formation through the intermolecular DoNA-p1:DoNA-p2 interactions. This peptide has some similarity to that designed by Fairman and colleagues to form fibers.[54] The fibers described herein are likely to contain tens to hundreds of thousands of peptide units (for a 1 μm long fiber, it is estimated it would contain $\sim$78 000 DoNA-GN$_1$ monomers). Similar phenomena are well-known for peptides that effectively harbor two complementary coiled-coil regions linked end to end, that is, without linkers.[55,56]

For the DoNA-GN system, a linker length of 4 residues appears to be the tipping point between these two behaviors, that is, the formation of discrete objects or fibers. This linker length is sufficiently flexible to allow nonfibrous closed structures to be formed, but too short to allow the formation of the smaller discrete objects; as a result, poorly defined colloid-scale particles are formed. From the size and the lower limit of the mass from AUC, these aggregates are likely to contain thousands of peptides (for a solid sphere $\sim$28 000 copies of DoNA-GN$_2$, and for a hollow sphere $\sim$1700 copies). At present, we cannot offer a more-detailed description of these particular structures, nor how they might be formed.

Although we have not conducted any specific kinetic studies, the assembly mechanism of some of these peptides is not straightforward: it seems that metastable states can get trapped kinetically. These states appear as broad distributions of high molecular weight species, that is, relative to the annealed states described next. However, most of the peptide constructs are able to access better-defined equilibrium ensembles, or even specific states, as follows. Assemblies formed from nonannealed samples can be unfolded by heating, and then refolded via controlled cooling. The resulting annealed samples are more helical, and have tighter distributions of lower molecular weight species, or even specific oligomeric states. For example, the constructs with the 6- and 8-residue linkers, this process leads to discrete nanoscale objects with 4 and 3 polypeptide chains each, respectively.

This property of annealing indicates that the various constructs have thermodynamically favored and defined states, that is, defined free-energy minima. This is despite the relative simplicity of their design. In turn, this offers new prospects for engineering discrete and potentially useful protein-like structures from this design approach. Thus, this study begins to pave the way in a component- or tecton-based approach to constructing self-assembling, linear, proteinogenic polypeptides of increasing complexity.[1,2] This could lead to new peptide- and protein-based assemblies and biomaterials and applications in protein engineering, bionanotechnology and synthetic biology.

ASSOCIATED CONTENT

ⓈSupporting Information

Supplementary CD, AUC, and SEC data; full disulfide exchange HPLC traces; WebLogo for linker selection; EM images and related width measurements of the fibers; additional modeling data. This material is available free of charge via the Internet at http://pubs.acs.org.

■ AUTHOR INFORMATION

Corresponding Author
E.H.C.Bromley@durham.ac.uk; D.N.Woolfson@bristol.ac.uk

Present Addresses
[#]Department of Physics, University of Durham, South Road, Durham DH1 3LE, U.K.
[¶]Department of Physics, Clarendon Laboratory, University of Oxford, Parks Road, Oxford OX1 3PU, U.K.

Notes
The authors declare no competing financial interest.

■ REFERENCES

(1) Bromley, E. H. C.; Channon, K.; Moutevelis, E.; Woolfson, D. N. ACS Chem. Biol. 2008, 3, 38−50.
(2) Channon, K.; Bromley, E. H. C.; Woolfson, D. N. Curr. Opin. Struct. Biol. 2008, 18, 491−498.
(3) Seeman, N. C. Annu. Rev. Biochem. 2010, 79, 65−87.
(4) Goodman, R. P.; Berry, R. M.; Turberfield, A. J. Chem. Commun. 2004, 1372−1373.
(5) He, Y.; Ye, T.; Su, M.; Zhang, C.; Ribbe, A. E.; Jiang, W.; Mao, C. D. Nature 2008, 452, 198−U41.
(6) Douglas, S. M.; Dietz, H.; Liedl, T.; Hogberg, B.; Graf, F.; Shih, W. M. Nature 2009, 459, 414−418.
(7) Rothemund, P. W. K. Nature 2006, 440, 297−302.
(8) Andersen, E. S.; Dong, M.; Nielsen, M. M.; Jahn, K.; Subramani, R.; Mamdouh, W.; Golas, M. M.; Sander, B.; Stark, H.; Oliveira, C. L. P.; Pedersen, J. S.; Birkedal, V.; Besenbacher, F.; Gothelf, K. V.; Kjems, J. Nature 2009, 459, 73−75.
(9) Omabegho, T.; Sha, R.; Seeman, N. C. Science 2009, 324, 67−71.
(10) Muscat, R. A.; Bath, J.; Turberfield, A. J. Nano Lett. 2011, 11, 982−987.
(11) Berg, J. M. Acc. Chem. Res. 1995, 28, 14−19.
(12) Pabo, C. O.; Peisach, E.; Grant, R. A. Annu. Rev. Biochem. 2001, 70, 313−340.
(13) Fallas, J. A.; O'Leary, L. E. R.; Hartgerink, J. D. Chem. Soc. Rev. 2010, 39, 3510−3527.
(14) Woolfson, D. N. Biopolymers 2010, 94, 118−127.
(15) Papapostolou, D.; Smith, A. M.; Atkins, E. D. T.; Oliver, S. J.; Ryadnov, M. G.; Serpell, L. C.; Woolfson, D. N. Proc. Natl. Acad. Sci. U.S.A. 2007, 104, 10853−10858.
(16) Grigoryan, G.; Kim, Y. H.; Acharya, R.; Axelrod, K.; Jain, R. M.; Willis, L.; Drndic, M.; Kikkawa, J. M.; DeGrado, W. F. Science 2011, 332, 1071−1076.
(17) Kuhlman, B.; Dantas, G.; Ireton, G. C.; Varani, G.; Stoddard, B. L.; Baker, D. Science 2003, 302, 1364−1368.
(18) Padilla, J. E.; Colovos, C.; Yeates, T. O. Proc. Natl. Acad. Sci. U.S.A. 2001, 98, 2217−2221.
(19) Sinclair, J. C.; Davies, K. M.; Venien-Bryan, C.; Noble, M. E. M. Nat. Nanotechnol. 2011, 6, 558−562.
(20) Brodin, J. D.; Ambroggio, X. I.; Tang, C. Y.; Parent, K. N.; Baker, T. S.; Tezcan, F. A. Nat. Chem. 2012, 4, 375−382.
(21) Fletcher, J. M.; Boyle, A. L.; Bruning, M.; Bartlett, G. J.; Vincent, T. L.; Zaccai, N. R.; Armstrong, C. T.; Bromley, E. H. C.; Booth, P. J.; Brady, R. L.; Thomson, A. R.; Woolfson, D. N. ACS Synth. Biol. 2012, 1, 240−250.

15466

dx.doi.org/10.1021/ja3053943 | J. Am. Chem. Soc. 2012, 134, 15457−15467

(22) Yoshizumi, A.; Fletcher, J. M.; Yu, Z. X.; Persikov, A. V.; Bartlett, G. J.; Boyle, A. L.; Vincent, T. L.; Woolfson, D. N.; Brodsky, B. *J. Biol. Chem.* **2011**, *286*, 17512−17520.

(23) Kotch, F. W.; Raines, R. T. *Proc. Natl. Acad. Sci. U.S.A.* **2006**, *103*, 3028−3033.

(24) Gauba, V.; Hartgerink, J. D. *J. Am. Chem. Soc.* **2008**, *130*, 7509−7515.

(25) Krizek, B. A.; Amann, B. T.; Kilfoil, V. J.; Merkle, D. L.; Berg, J. M. *J. Am. Chem. Soc.* **1991**, *113*, 4518−4523.

(26) Kim, C. A.; Berg, J. M. *Nat. Struct. Biol.* **1996**, *3*, 940−945.

(27) Woolfson, D. N. *Adv. Protein Chem.* **2005**, *70*, 79−112.

(28) Crick, F. H. C. *Acta Crystallogr.* **1953**, *6*, 689−697.

(29) Lupas, A. N.; Gruber, M. *Adv. Protein Chem.* **2005**, *70*, 37−78.

(30) Moutevelis, E.; Woolfson, D. N. *J. Mol. Biol.* **2009**, *385*, 726−732.

(31) Steinkruger, J. D.; Woolfson, D. N.; Gellman, S. H. *J. Am. Chem. Soc.* **2010**, *132*, 7586−7588.

(32) Harbury, P. B.; Zhang, T.; Kim, P. S.; Alber, T. *Science* **1993**, *262*, 1401−1407.

(33) O'Shea, E. K.; Lumb, K. J.; Kim, P. S. *Curr. Biol.* **1993**, *3*, 658−667.

(34) Nautiyal, S.; Woolfson, D. N.; King, D. S.; Alber, T. *Biochemistry* **1995**, *34*, 11645−11651.

(35) Bromley, E. H. C.; Sessions, R. B.; Thomson, A. R.; Woolfson, D. N. *J. Am. Chem. Soc.* **2009**, *131*, 928−930.

(36) Reinke, A. W.; Grant, R. A.; Keating, A. E. *J. Am. Chem. Soc.* **2010**, *132*, 6025−6031.

(37) McClain, D. L.; Woods, H. L.; Oakley, M. G. *J. Am. Chem. Soc.* **2001**, *123*, 3151−3152.

(38) Gurnon, D. G.; Whitaker, J. A.; Oakley, M. G. *J. Am. Chem. Soc.* **2003**, *125*, 7518−7519.

(39) Pandya, M. J.; Cerasoli, E.; Joseph, A.; Stoneman, R. G.; Waite, E.; Woolfson, D. N. *J. Am. Chem. Soc.* **2004**, *126*, 17016−17024.

(40) Zaccai, N. R.; Chi, B.; Thomson, A. R.; Boyle, A. L.; Bartlett, G. J.; Bruning, M.; Linden, N.; Sessions, R. B.; Booth, P. J.; Brady, R. L.; Woolfson, D. N. *Nat. Chem. Biol.* **2011**, *7*, 935−941.

(41) Bromley, E. H. C.; Kuwada, N. J.; Zuckermann, M. J.; Donadini, R.; Samii, L.; Blab, G. A.; Gemmen, G. J.; Lopez, B. J.; Curmi, P. M. G.; Forde, N. R.; Woolfson, D. N.; Linke, H. *HFSP J.* **2009**, *3*, 204−212.

(42) de la Torre, J. G.; Huertas, M. L.; Carrasco, B. *Biophys. J.* **2000**, *78*, 719−730.

(43) Offer, G.; Hicks, M. R.; Woolfson, D. N. *J. Struct. Biol.* **2002**, *137*, 41−53.

(44) Demeler B. *UltraScan—A Comprehensive Data Analysis Software Package for Analytical Ultracentrifugation Experiments*; The University of Texas Health Science Center at San Antonio: San Antonio, TX, 2005

(45) M., L. T.; B.D., S.; T.M., R.; S.I., P. *Analytical Ultracentrifugation in Biochemistry and Polymer Science*; The Royal Society of Chemistry, Cambridge, 1992.

(46) Testa, O. D.; Moutevelis, E.; Woolfson, D. N. *Nucleic Acids Res.* **2009**, *37*, D315−D322.

(47) Crooks, G. E.; Hon, G.; Chandonia, J. M.; Brenner, S. E. *Genome Res.* **2004**, *14*, 1188−1190.

(48) Humphrey, W.; Dalke, A.; Schulten, K. *J. Mol. Graphics* **1996**, *14*, 33−38.

(49) Litowski, J. R.; Hodges, R. S. *J. Pept. Res.* **2001**, *58*, 477−492.

(50) Gonzalez, L.; Woolfson, D. N.; Alber, T. *Nat. Struct. Biol.* **1996**, *3*, 1011−1018.

(51) Nicolas, E.; Pedroso, E.; Giralt, E. *Tetrahedron Lett.* **1989**, *30*, 497−500.

(52) Gribbon, C.; Channon, K. J.; Zhang, W. J.; Banwell, E. F.; Bromley, E. H. C.; Chaudhuri, J. B.; Oreffo, R. O. C.; Woolfson, D. N. *Biochemistry* **2008**, *47*, 10365−10371.

(53) Papapostolou, D.; Bromley, E. H. C.; Bano, C.; Woolfson, D. N. *J. Am. Chem. Soc.* **2008**, *130*, 5124−5130.

(54) Wagner, D. E.; Phillips, C. L.; Ali, W. M.; Nybakken, G. E.; Crawford, E. D.; Schwab, A. D.; Smith, W. F.; Fairman, R. *Proc. Natl. Acad. Sci. U.S.A.* **2005**, *102*, 12656−12661.

(55) Pandya, M. J.; Spooner, G. M.; Sunde, M.; Thorpe, J. R.; Rodger, A.; Woolfson, D. N. *Biochemistry* **2000**, *39*, 8728−8734.

(56) Woolfson, D. N.; Mahmoud, Z. N. *Chem. Soc. Rev.* **2010**, *39*, 3464−3479.